

光学学报

基于傅里叶变换光学系统的动态多光束干涉光刻

叶燕^{1,2}, 马亚骥^{1,2}, 宋志^{1,2}, 路畅^{1,2}, 许宜申^{1,2*}, 陈林森^{1,2**}

¹苏州大学光电科学与工程学院, 苏州纳米科技协同创新中心, 江苏 苏州 215006;

²苏州大学江苏省先进光学制造技术重点实验室, 教育部现代光学技术重点实验室, 江苏 苏州 215006

摘要 变参量微纳结构在二维平面内交叉、分段排布可以实现超表面器件的多路复用和多功能集成。为实现交叉、分段变参量微纳结构的干涉制备,提出了孔径光阑与相位元件联合调制的傅里叶变换光学系统。利用透镜的傅里叶变换特性和相位元件衍射光线的几何传播特性,阐明了傅里叶成像面上交叉、分段分布的多干涉光场的生成方法与调控规律。同时,针对目标分布的变参量微纳结构,反演设计了多像素孔径光阑与基于光栅和变参量光栅的相位元件,实验获得了交叉、分段分布的多干涉光场。将多干涉光场与微缩投影结合可制备分段排布的纳米光栅。将动态调控的多干涉光场分时复用可制备分段排布的变参量纳米光栅。

关键词 光学设计; 相位调制; 4f光学系统; 空间变参量; 干涉光刻

中图分类号 O438.2; TH691.9

文献标志码 A

DOI: 10.3788/AOS221892

1 引言

超表面利用空间变参量微纳结构对光场振幅、相位等参数进行调控或变换,可产生单一定参量微纳结构无法实现的新现象、新功能和器件,在超透镜^[1-4]、隐形斗篷^[5-6]、彩色滤光片^[7-9]、全息^[10-13]和光束整形^[14-15]等领域中取得了令人瞩目的研究进展。为满足光电器件日益增长的多功能、集成化需求,将变参量微纳结构在二维平面内交叉、分段排列^[16-22],实现超表面器件的多功能集成或多路复用成为了新的发展趋势。

空间变参量微纳结构的快速制备是实现超表面器件规模化应用的关键。在现有工艺中,投影光刻与干涉光刻是实现微纳结构快速制备的有效手段^[23]。投影光刻利用紫外光照明将几何图案从光掩模转移到光致抗蚀剂上,通过高分辨率掩模版实现变参量微纳结构的快速制备。She等^[24]利用步进投影光刻设备分步分区曝光,通过限定圆柱直径变化范围、固定圆柱间相邻边距的方法,制备了幅面为314 mm²的空间变参量圆柱点阵结构。采用相同的方法,Colburn等^[25]扩大了圆柱直径和圆柱间相邻边距的变化范围,空间变参量圆柱点阵的幅面减小为100 mm²。因此,步进投影光刻可制备的微纳结构的幅面大小严重受到其参量变化范围的制约。

干涉光刻所制备的结构参量固定,为实现变参量微纳结构的制备,主要通过调节相干光束的光强分布、

相干夹角等方法改变微纳结构的轮廓、周期等参量^[26-31],此类方法调控的微纳结构参量变化范围窄、精度低,且光学系统构建十分复杂。陈林森等^[32-38]将干涉光刻与投影光刻结合,提出了相位调制的傅里叶变换光学系统,利用衍射光栅作为相位元件调制入射光,在系统成像面内形成干涉光场,通过相位元件的平移、旋转即可实现干涉光场空间频率、取向的连续调控,实现了微纳光栅的在线逐像素制备,355 nm工作波长下可制备的最小线宽为95 nm。在此基础上,Ye等^[39-40]采用复杂相位元件分段调制入射光,实现了微纳结构多像素的同时制备,但失去了相位元件相对运动带来的调控维度。

为实现多干涉光场的分布区域和光场参量的分离调控,本文提出了孔径光阑、相位元件联合调制的傅里叶变换光学系统,阐明在多像素孔径光阑调制入射光振幅时,分别利用相位元件、变参量相位元件±1级衍射光的传播特性生成、调控多干涉光场的方法。在此基础上,针对所需空间排布的变参量微纳结构,反演设计了孔径光阑与光栅相位元件和孔径光阑与变参量光栅相位元件,实验获得了分段分布的多干涉光场和交叉分布的变参量多干涉光场。采用分段分布的多干涉光场微缩投影曝光,在光刻胶表面实现了分段排布的纳米光栅的多像素制备。采用分时复用动态调控的多干涉光场获得了分段排布的像素化变参量纳米光栅。理论与实验研究结果表明,该联合调制的傅里叶变换

收稿日期: 2022-10-28; 修回日期: 2022-11-23; 录用日期: 2022-12-02; 网络首发日期: 2023-01-04

基金项目: 国家自然科学基金(62075149,61575132)、江苏省自然科学基金(BK20201406)、江苏省高校优势学科建设(PAPD)

通信作者: *xys2001@suda.edu.cn; **lschen@suda.edu.cn

光学系统可为分段、交叉分布的变参量微纳结构的多像素制备提供工艺基础。

2 傅里叶变换光学系统及其调制原理

孔径光阑和相位元件联合调制的傅里叶变换光学

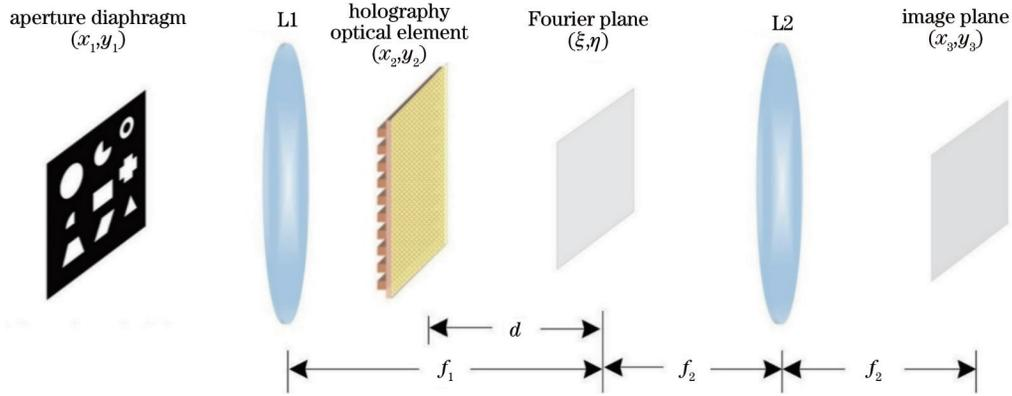


图 1 孔径光阑和相位元件调制的傅里叶变换光学系统示意图

Fig. 1 Schematic diagram of optical Fourier transform system modulated by aperture diaphragm and phase element

准直平行后的激光垂直照射于孔径光阑,经孔径光阑调制振幅后由透镜 L1 会聚至相位元件,相位元件生成透射衍射光后会聚于傅里叶频谱面形成多个频谱斑。此时,傅里叶频谱面上的频谱斑将作为相干次波源,经第二傅里叶变换透镜 L2 变换为多束平行光,在傅里叶成像面处发生干涉。

设孔径光阑平面、相位元件平面、傅里叶频谱面和

系统如图 1 所示,该系统采用傅里叶变换光路,在第一傅里叶变换透镜前放置孔径光阑,在第一傅里叶变换透镜与傅里叶频谱面之间放置相位元件。

像面的坐标平面分别为 (x_1, y_1) 、 (x_2, y_2) 、 (ξ, η) 和 (x_3, y_3) 。设孔径光阑的透射函数为 $\sum_{i=1}^n a_i(x_1, y_1)$, 相位元件的透射函数为 $t(x_2, y_2)$, 根据衍射受限系统的成像性质与线性空不变特性^[38], 傅里叶频谱面的光场可以表示为

$$U(\xi, \eta) = c \sum_{i=1}^n A_i(\xi, \eta) * T(\xi, \eta) = c \iint \sum_{i=1}^n a_i(x_1, y_1) \exp\left(-j2\pi \frac{\xi x_1 + \eta y_1}{\lambda f_1}\right) dx_1 dy_1 * \iint t(x_2, y_2) \exp\left(-j2\pi \frac{\xi x_2 + \eta y_2}{\lambda d}\right) dx_2 dy_2, \quad (1)$$

式中: $A_i(\xi, \eta)$ 为 $a_i(x_1, y_1)$ 的傅里叶变换, 其傅里叶变换尺度为 λf_1 ; $T(\xi, \eta)$ 为相位元件透射函数 $t(x_2, y_2)$ 的傅里叶变换, 傅里叶变换尺度为 λd ; * 为卷积符号。由

于傅里叶频谱面是第二傅里叶变换透镜的前焦面, 故傅里叶成像面上的光场分布为 $U(\xi, \eta)$ 的傅里叶变换, 傅里叶变换尺度为 λf_2 , 即

$$U(x_3, y_3) = c \iint \sum_{i=1}^n A_i(\xi, \eta) \exp\left(-j2\pi \frac{\xi x_3 + \eta y_3}{\lambda f_2}\right) d\xi d\eta * \iint T(\xi, \eta) \exp\left(-j2\pi \frac{\xi x_3 + \eta y_3}{\lambda f_2}\right) d\xi d\eta. \quad (2)$$

将式(1)代入式(2)中简化得到的成像面光场的表达式为

$$U(x_3, y_3) = c^n \sum_{i=1}^n a_i\left(-\frac{f_1}{f_2} x_3, -\frac{f_1}{f_2} y_3\right) t\left(-\frac{d}{f_2} x_3, -\frac{d}{f_2} y_3\right), \quad (3)$$

式中: $a_i\left(-\frac{f_1}{f_2} x_3, -\frac{f_1}{f_2} y_3\right)$ 和 $t\left(-\frac{d}{f_2} x_3, -\frac{d}{f_2} y_3\right)$ 为孔径光阑和相位元件透射函数的两次傅里叶变换结果, 是孔径光阑平面和相位元件平面透射函数的镜像缩放。由此可见, 傅里叶成像面的输出光场由孔径光阑的孔径分布和相位元件的透射衍射共同决定, 两者的

任意变化均可调控输出光场。

2.1 全息光学相位元件

当相位元件为仅生成 ± 1 级衍射光的全息光学元件时, 孔径光阑和相位元件联合调制的傅里叶变换光学系统的等效几何传播光路如图 2(a) 所示, 准直平行光经孔径光阑调制形成 4 束平行光, 经会聚、衍射和变

换后在傅里叶成像面两两相干,形成相干光场 A 和 B。

根据式(3),输出光场可表示为

$$U(x_3, y_3) = c'' \left\{ \left[a_1 \left(-\frac{f_1}{f_2} x_3, -\frac{f_1}{f_2} y_3 \right) + b_1 \left(-\frac{f_1}{f_2} x_3, -\frac{f_1}{f_2} y_3 \right) \right] t_{+1} \left(-\frac{d}{f_2} x_3, -\frac{d}{f_2} y_3 \right) + \left[a_2 \left(-\frac{f_1}{f_2} x_3, -\frac{f_1}{f_2} y_3 \right) + b_2 \left(-\frac{f_1}{f_2} x_3, -\frac{f_1}{f_2} y_3 \right) \right] t_{-1} \left(-\frac{d}{f_2} x_3, -\frac{d}{f_2} y_3 \right) \right\} \quad (4)$$

由式(4)可知,孔径光阑可调控相应级次透射光场在傅里叶成像面上的分布区域,从而调控透射子光场间的叠加相干。设入射波波长为 λ ,相位元件的空间频率为 F_0 ,根据光线可逆原理,成像于光轴的光线传播原理如图2(b)所示。由垂直入射时的光栅方程可知 $\sin \theta = F_0 \lambda$,而近轴近似条件下 $\tan \theta = \sin \theta$,则有 $h_2 = d \tan \theta = d \lambda F_0$ 。根据几何相似原理 $d/f_1 = h_2/h_1$,

则 $h_1 = h_2 f_1/d = \lambda f_1 F_0$,即若孔径光阑面的光线偏离光轴距离 $h_1 = \lambda f_1 F_0$,则在成像面中该光线将成像于光轴。因此,可将空间光阑面上成像于光轴的光线作为标准光线,该光线偏离光轴的距离作为标准距离。当光线向上偏离标准光线距离 d_1 时,根据几何相似原理,有 $d_2/d_3 = d/f_2$ 和 $d_1/d_2 = f_1/d$,则其在成像面向下偏离光轴距离 $d_3 = d_1 f_2/f_1$ 。

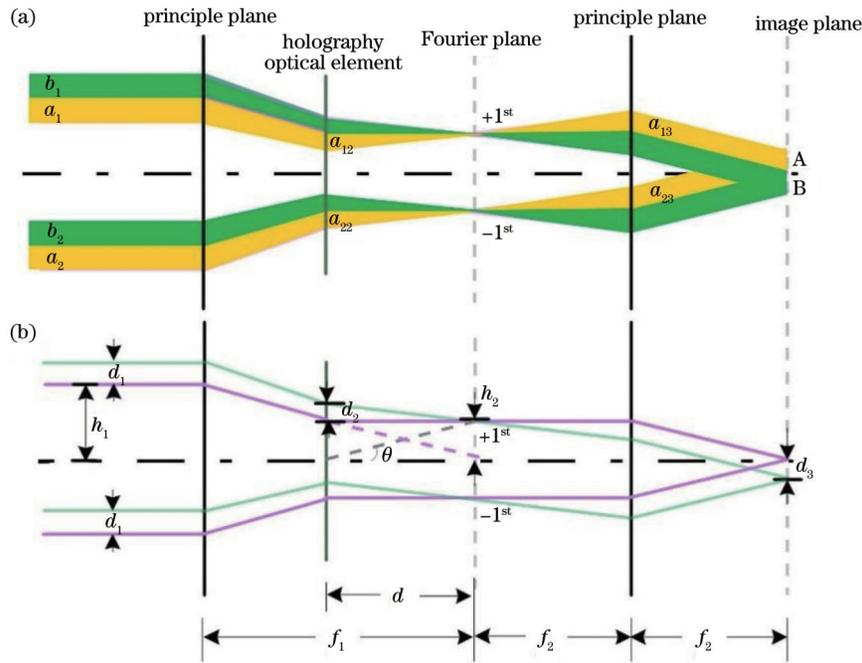


图 2 傅里叶调制光学系统的等效几何传播光路和成像于光轴的光线的几何传播光路。(a) 等效几何传播光路;(b) 成像于光轴的光线的几何传播光路

Fig. 2 Equivalent geometrical light path for modulated Fourier transform system and geometrical light path of light imaged on optical axis. (a) Equivalent geometrical light path; (b) geometrical light path of light imaged on optical axis

因此,通过孔径光阑可调控成像面的透射光场,如图2(a)所示:光束 a_1 、 a_2 向下偏离对称标准光线相同的距离,两者在傅里叶成像面上叠加相干,形成的干涉光场A分布在成像面光轴上方;光束 b_1 、 b_2 向上偏离对称标准光线相同的距离,两者在成像面上叠加相干,形成的干涉光场B分布在成像面光轴下方;光束 a_1 、 b_2 位于对称标准光线的两侧,两者形成的光场在成像面光轴的两侧,相邻但不叠加。

当 ± 1 级衍射光的对应光场在傅里叶成像面上叠加相干时,对应干涉光场的分布区域是对应孔径光阑

的 f_1/f_2 倍,干涉光场的空间频率为 $2dF_0/f_2$ 。因此,当相位元件沿光轴在透镜L1与傅里叶频谱面之间平移时,即 d 在 $0 \sim f_1$ 之间变化时,傅里叶成像面的光场分布区域恒定,相干光场的空间频率在 $0 \sim 2F_0 f_1/f_2$ 之间变化。

2.2 变参量全息相位元件

当像素化全息光学元件作为相位元件时,如图3(a)所示,准直平行光经孔径光阑调制形成4束平行光,在傅里叶成像面两两相干,形成相干光场A和B。根据式(3),输出光场可以表示为

$$U(x_3, y_3) = c'' \left[a_1 \left(-\frac{f_1}{f_2} x_3, -\frac{f_1}{f_2} y_3 \right) t_{+1a} \left(-\frac{d}{f_2} x_3, -\frac{d}{f_2} y_3 \right) + a_2 \left(-\frac{f_1}{f_2} x_3, -\frac{f_1}{f_2} y_3 \right) t_{-1a} \left(-\frac{d}{f_2} x_3, -\frac{d}{f_2} y_3 \right) + b_1 \left(-\frac{f_1}{f_2} x_3, -\frac{f_1}{f_2} y_3 \right) t_{+1b} \left(-\frac{d}{f_2} x_3, -\frac{d}{f_2} y_3 \right) + b_2 \left(-\frac{f_1}{f_2} x_3, -\frac{f_1}{f_2} y_3 \right) t_{-1b} \left(-\frac{d}{f_2} x_3, -\frac{d}{f_2} y_3 \right) \right], \quad (5)$$

式中： t_{+1a} 、 t_{-1a} 和 t_{+1b} 、 t_{-1b} 分别为空间频率为 F_0 和 F_1 的全息光学元件的 +1、-1 级透射衍射。由式(5)可知，傅里叶成像面光场由孔径光阑的孔径分布和全息光学元件的透射光场共同决定，可通过调控孔径分布实现 +1 级与 -1 级衍射光场的两两叠加相干。图 3(a) 对应的等效几何光路与图 2(b) 类似：当孔径光阑面光线偏离光轴标准距离 $h_i = \lambda f_1 F_i (i = 0, 1)$ 时，光线在成像面成像于光轴；若孔径光阑面光线向上偏离标准光线距离 d_1 ，则光线在成像面向下偏离光轴距离 $d_3 = d_1 f_2 / f_1$ 。当相位元件在透镜 L1 与傅里叶频谱面之间沿光轴平移时，即 d 在 $0 \sim f_1$ 之间变化时，孔径光阑在全息光学元件上投影的高度与大小按 d/f_1 的倍率随之

发生线性变化。

为避免相位元件像素分布对透射光场分布区域的影响，根据相位元件沿光轴平移时孔径光阑在全息光学元件上投影的高度与大小的线性变化，设计出变参量全息光学元件的像素分布，如图 3(b) 所示。可以看出，像素呈扇形对称分布，对称中心落在光学系统的光轴上，随着像素位置远离对称中心，相应像素尺寸线性增大。当孔径光阑投影在全息光学元件不同的像素位置时，如图 3(c) 所示，若相位元件沿光轴平移，则孔径光阑在相位元件上的投影同步增大或缩小，投影高度同步向相位元件中心远离或收缩，即相位元件沿光轴的相对运动不影响孔径光阑对其透射光场的选择与调制。

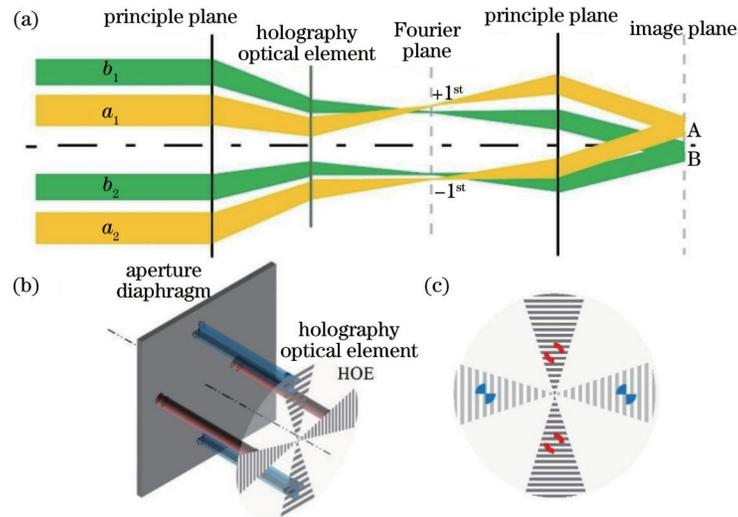


图 3 孔径光阑和变参量相位元件联合调制的傅里叶变换光学系统。(a) 等效几何传播光路；(b) 孔径光阑在变参量相位元件上的成像示意图；(c) 孔径光阑与扇区光栅对应关系示意图

Fig. 3 Fourier transform system jointly modulated by aperture diaphragm and space-variant phase element. (a) Equivalent geometrical light path; (b) schematic diagram of aperture diaphragm imaged on space-variant grating; (c) schematic diagram of symmetric distribution for aperture diaphragm and grating pixel

孔径光阑和相位元件联合调制的傅里叶变换光学系统可实现多干涉光场的生成与动态调控，其中相位元件的作用是确立每个子光场的光场参量，孔径光阑的作用是调控每个子光场的分布区域与叠加相干情况：当仅相位元件沿光轴平移时，光场空间频率随之发生变化，光场的分布区域与叠加情况不变；当仅孔径光阑发生变化时，光场的分布区域、相干组合方式均可按需变化；当相位元件旋转时，若孔径光阑同步旋转，则多干涉光场仅取向发生变化。因此，孔径光阑与相位元件联合调制的傅里叶变换光学系统具有很高的可

控性。

3 多像素微纳光场反演设计

3.1 孔径光阑与全息光学相位元件

采用所设计的孔径光阑和全息光学相位元件调制的傅里叶变换光学系统，根据多干涉光场的生成与调控原理，通过反演设计孔径光阑与相位元件可实现定制化光场的生成与调制，从而实现微纳结构的在线制备。如图 4(a) 所示的微米光栅，该微米光栅在二维平面内分为 9 个子像素，每 3 个子像素的尺寸、像素内填

充的光栅结构的空空间频率相同,其中:空间频率为 176 lp/mm 的微米结构的像素尺寸为 1.71 mm×1.71 mm;空间频率为 222 lp/mm 的微米结构的像素尺寸为 0.90 mm×0.90 mm;空间频率为 302 lp/mm 的微米结构的像素尺寸为 0.33 mm×0.33 mm。鉴于成像面透射光场与相位元件透射光场的镜像缩放关

系,选择消 0 级光光栅作为相位元件。根据孔径光阑与全息光学元件联合调制时的多干涉光场生成与调控原理,反演设计的孔径光阑如图 4(b)~(d)所示,在垂直于光栅栅线方向,每 2 个矩形孔径组成一组孔径光阑,每个矩形孔径中心相对对称中心偏移不同的距离。

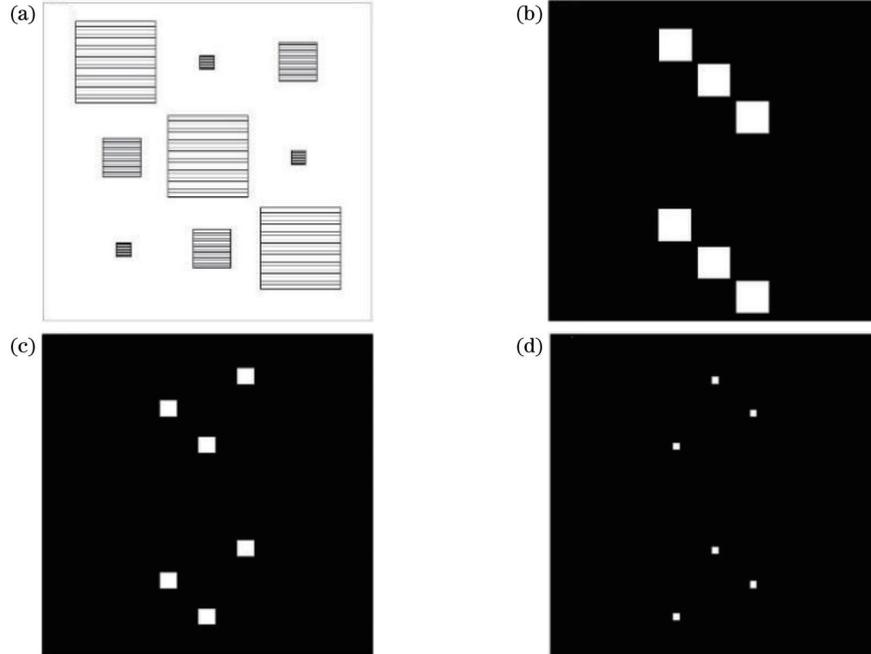


图 4 二维平面内分段分布的微米光栅及其反演设计的孔径光阑示意图。(a)三种微米光栅二维平面内分段分布示意图;(b)~(d)三种微米光栅分段分布的反演设计的孔径光阑
Fig. 4 Schematic diagram of planar segmented micro-grating and inversely designed aperture diaphragms. (a) Schematic diagram of planar segmented micro-grating with three frequencies; (b)~(d) inversely designed aperture diaphragms for segmented micro-grating with three frequencies

当傅里叶变换光学系统采用波长为 355 nm 的紫外光照明,傅里叶变换透镜的焦距均为 72.2 mm 时,傅里叶成像面与孔径平面间的成像放大倍率为 1,此时孔径光阑的尺寸与成像面的像素尺寸相同。当光栅相位元件的空间频率为 200 lp/mm 时,根据 $h_1 = \lambda f_1 F_0$ 计算得到孔径光阑面内标准光线偏离光轴的标准距离为 ± 5.126 mm,若成像面内各像素偏离光轴的距离为 $d_3 = 2$ mm,则各孔径光阑中心相对标准光线的偏移量为 $d_1 = d_3 f_1 / f_2 = d_3 = 2$ mm。为在傅里叶成像面上获得空间频率 F_1 分别为 176、222、302 lp/mm 的微米光栅,光栅相位元件偏离傅里叶频谱面的距离 $[d = F_1 f_2 / (2F_0)]$ 经计算分别为 31.77、40.13、54.46 mm,从而反演得到孔径光阑分布与光栅相位元件的位置参数,如表 1 所示。

上述孔径光阑与光轴交点的坐标为 $(0, 0)$,若边长为 b 的矩形光阑的中心与光轴的距离为 r ,相邻光阑中心的横纵坐标偏移为 c ,则每组孔径光阑内包含的矩形光阑中心坐标可表示为 $\begin{cases} x_n = nc \\ y_n = \pm r - nc \end{cases} (n = -1, 0, 1)$,

此时孔径光阑的透射光场可以表示为

$$\sum_{n=-1}^1 b \text{rect}\left(\frac{x-x_n}{b}, \frac{y-y_n}{b}\right) = \begin{cases} 1, & |x| \leq \frac{b}{2} \text{ and } |y| \leq \frac{b}{2}, \\ 0, & \text{otherwise} \end{cases} \quad (6)$$

式中: $\text{rect}(\cdot)$ 为矩形函数。光栅相位元件的透射光场为

$$t(x_2, y_2) = \exp(j2\pi F_0 y_2) + \exp(-j2\pi F_0 y_2) \quad (7)$$

依据式(4),孔径光阑与相位元件联合调制的傅里叶变换光学系统在傅里叶频谱面和傅里叶成像面上的光场分布如图 5 所示。当相位元件分别偏离傅里叶频谱面相应距离,与 3 组孔径光阑联合调制傅里叶变换光学系统时,其在傅里叶频谱面的光场分布如图 5(a)~(c)所示,该光场为孔径光阑和相位元件透射光场傅里叶变换的卷积,呈现傅里叶频谱斑分布。相应的傅里叶成像面的光场输出如图 5(d)~(f)所示。可以发现:在系统的成像面上同时生成了 3 个分段分布的干涉光场,干涉光场的分段分布与目标微米光栅的像素排布相同;每个干涉光场内包含空间频率、取向一致的干涉

表 1 孔径光阑与相位元件对应参数

Table 1 Corresponding parameters for aperture diaphragms and phase elements

Target pixel		Aperture diaphragm		Holography optical element	
Frequency / (lp·mm ⁻¹)	Pixel diameter / (mm × mm)	Central position /mm		Pixel diameter / (mm × mm)	Frequency / (lp·mm ⁻¹) Distance / mm
176	1.71 × 1.71	(-2.000 mm, 7.126 mm), (-2.000 mm, 3.126 mm), (0, 5.126 mm), (0, -5.126 mm), (2.000 mm, 3.126 mm), (2.000 mm, -7.126 mm)		1.71 × 1.71	31.77
222	0.90 × 0.90	(-2.000 mm, 5.126 mm), (-2.000 mm, -5.126 mm), (0, 3.126 mm), (0, -7.126 mm), (2.000 mm, -3.126 mm), (2.000 mm, 7.126 mm)		0.90 × 0.90	200 40.13
302	0.33 × 0.33	(-2.000 mm, 3.126 mm), (-2.000 mm, -7.126 mm), (0, 7.126 mm), (0, -3.126 mm), (2.000 mm, 5.126 mm), (2.000 mm, -5.126 mm)		0.33 × 0.33	54.46

条纹;改变孔径光阑和平移相位元件后,对应多干涉光场的分布区域和光场内干涉条纹的空间频率也会发生改变。由于干涉光场的分布区域是对应孔径光阑的 f_1/f_2 倍,故图 5(d)~(f)所示干涉光场的区域尺寸分别为 1.71 mm × 1.71 mm、0.90 mm × 0.90 mm、

0.33 mm × 0.33 mm。干涉光场的空间频率为 $2dF_0/f_2$,故对应光场内干涉条纹的空间频率分为 176、222、302 lp/mm。各干涉光场在二维平面内相互垂直方向的偏移量均为 2 mm。理论分析结果表明,在傅里叶成像面上获得的多干涉光场满足设计需求。

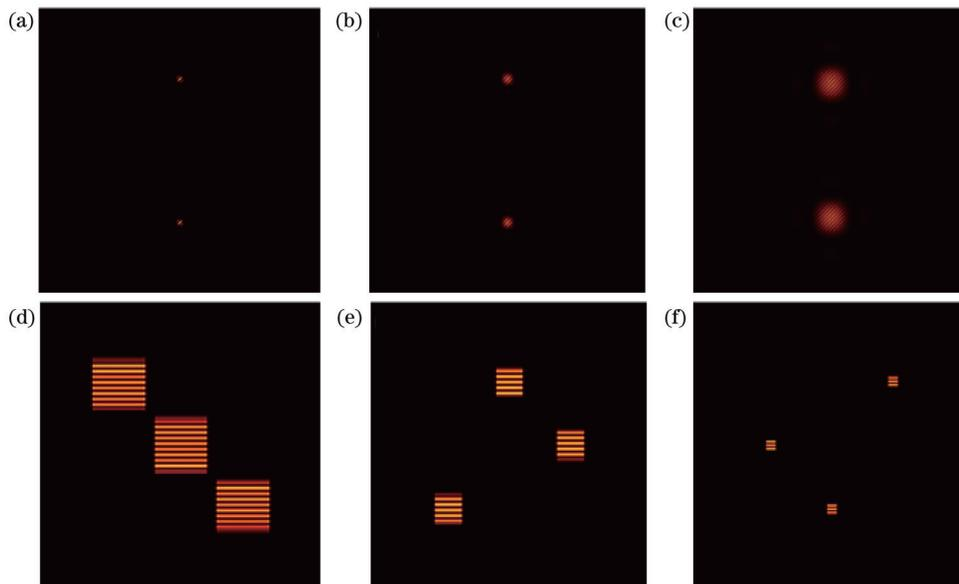


图 5 傅里叶频谱面和成像面上的光场分布。(a)~(c)傅里叶频谱面上的光场分布;(d)~(f)傅里叶成像面上的光场分布

Fig. 5 Light field distributions on Fourier spectrum plane and imaging plane. (a)~(c) Light field distribution on Fourier spectrum plane; (d)~(f) light field distribution on Fourier imaging plane

因此,当利用多像素孔径光阑和全息光学元件联合调控傅里叶变换光路时,根据其多干涉光场的生成与调控方法,反演设计孔径光阑和相位元件,可实现定制化分段分布的多干涉光场。同时,对相位元件的相对运动进行调控可动态调控多干涉光场内的结构参量。

3.2 孔径光阑与变参量全息光学相位元件

采用所设计的孔径光阑和像素化全息光学元件联合调制的傅里叶变换光学系统,根据多干涉光场的生

成与调控原理,通过反演设计孔径光阑与相位元件可实现变参量干涉光场的生成与调制,从而实现微纳结构的在线制备。如图 6(a)所示,8种取向的微米光栅在圆、环和分扇区内交叉分布,光栅取向的旋转角为 22.5° ,结构中圆、环像素关于圆心对称。由于所需结构为不同取向的微米光栅,故根据孔径光阑与变参量全息光学元件联合调制的多干涉光场生成与调控的原理,采用像素化分布、变取向的消 0 级光栅作为相位元件。如图 6(b)所示,该变参量光栅相位元件包含 8

种取向的光栅,是由顶角为 $\Delta k\pi = \pi/8$ 的扇形区域在 $0 \sim 2\pi$ 内连续变化步长 $\Delta k\pi$ 旋转得到的组合图案,该变

参量光栅相位元件的透射光场可以表示为

$$t(x_2, y_2) = \sum_{n=1}^N \left\{ \exp[j2\pi F_0(x_2 \sin \theta_n + y_2 \cos \theta_n)] + \exp[-j2\pi F_0(x_2 \sin \theta_n + y_2 \cos \theta_n)] \right\} \text{circ}\left(\frac{\sqrt{x_2^2 + y_2^2}}{r_0}\right), \quad (8)$$

式中: $x_2 \tan(\theta_n - \Delta k\pi/2) < y_2 < x_2 \tan(\theta_n + \Delta k\pi/2)$;

$\text{circ}(\cdot)$ 为不可分离变量的二元函数。

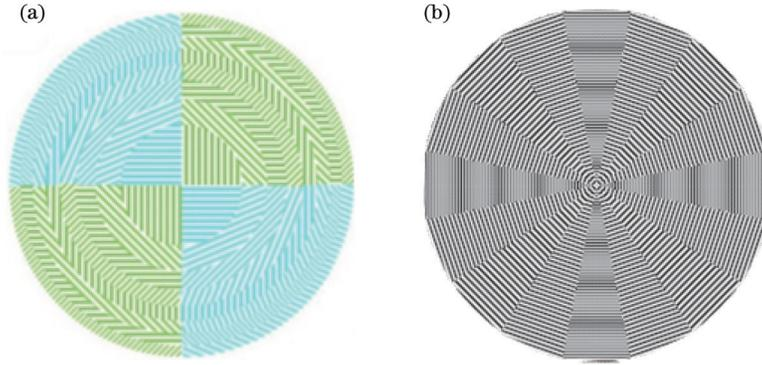


图 6 空间取向光栅结构和变取向光栅相位元件示意图。(a)空间取向光栅结构示意图;(b)变参量光栅相位元件示意图

Fig. 6 Structural diagram of spatial orientation grating and schematic diagram of phase element with orientation-variant grating.

(a) Structural diagram of spatial orientation grating; (b) schematic diagram of phase element with orientation-variant grating

在傅里叶变换光学系统中,傅里叶变换透镜的焦距相同,而图 6(a)中像素分布关于圆心对称,故将其圆心置于成像面的光轴上,此时孔径光阑的尺寸与成像面上像素的尺寸完全相同。以图 6(a)中水平栅线方向的所有微米光栅为目标,为实现其对应的圆、环分布下的多干涉光场,利用相位元件中相同取向的子扇区反演设计的孔径光阑,如图 7(a)所示。孔径光阑的扇区方向与相位元件子扇区相同,孔径光阑像素按照目标光栅分布方式组合,两组光阑在垂直于光栅栅线的方向对称分布。相应的傅里叶成像面上的光场分布如图 7(d)所示,生成的多个干涉光场分布区域和干涉光场内条纹取向与设计需求相符。

以此为基础,若要实现不同取向的多干涉条纹光场同时输出,则可根据同取向干涉光场的分布反演设计孔径光阑的组合,再将不同取向干涉光场下的孔径光阑按对应扇区组合。利用上述方法,反演设计的孔径光阑如图 7(b)所示,对称光阑中心连线垂直于光栅栅线,每组光阑之间的夹角为 22.5° 。孔径光阑面与光学系统光轴的交点坐标为 $(0, 0)$,若各孔径光阑圆心与光轴间的距离为 h ,光阑第 n 个圆的半径为 r_n ,则孔径光阑中心可以表示为 $\begin{cases} x_n = h \sin \theta_n \\ y_n = h \cos \theta_n \end{cases}$,其中 $n \in [0, N]$ 和 $\theta_n = \sum_{n=1}^N \frac{n\pi}{8}$,此时多像素孔径光阑的透射光场为

$$\sum_{n=0}^N \text{circ}\left(\frac{\sqrt{(x-x_n)^2 + (y-y_n)^2}}{r_n + 1 - r_n}\right) = \begin{cases} 1, & \sqrt{x^2 + y^2} \leq r_n, \\ 0, & \text{otherwise} \end{cases} \quad (9)$$

其中 $xy < 0$ 和 $r_0 = 0$ 对应二四象限的对角扇环透光区域。利用该孔径光阑与变参量光栅元件联合调制的傅里叶光学系统,依据式(5),其在成像面上的光场分布如图 7(e)所示。可以发现:多干涉光场的分布区域组成二分之一圆,包含 8 个干涉光场,每个干涉光场内产生干涉条纹,相邻光场内的条纹夹角为 22.5° ,形成 2π 的取向变化,该模拟光场的像素分布和干涉条纹取向变化与图 6(a)中的所需结构完全相同。

根据多干涉光场的生成原理,再次改变孔径光阑设计,如图 7(c)所示。利用该孔径光阑与变参量光栅元件联合调制傅里叶光学系统,其在成像面上的光场如图 7(f)所示。可以发现:光场分布区域为圆形,整个圆形区域内包含 16 个干涉光场,其中 8 个干涉光场形成交叉分布的子扇区,内圆区域干涉光场生成的条纹取向一致;每个子扇区中相邻圆环内干涉光场生成的条纹夹角为 22.5° ,形成 2π 的取向变化。与图 7(e)相比,对应子扇区下光栅的取向不同。

因此,当利用多像素孔径光阑与变参量全息光学元件联合调控傅里叶变换光路时,可根据其多干涉光场的生成与调控方法,反演设计孔径光阑与变参量相位元件,实现定制化交叉、分段分布的多干涉光场。同时,可通过孔径光阑的变化调制多干涉光场的空间分

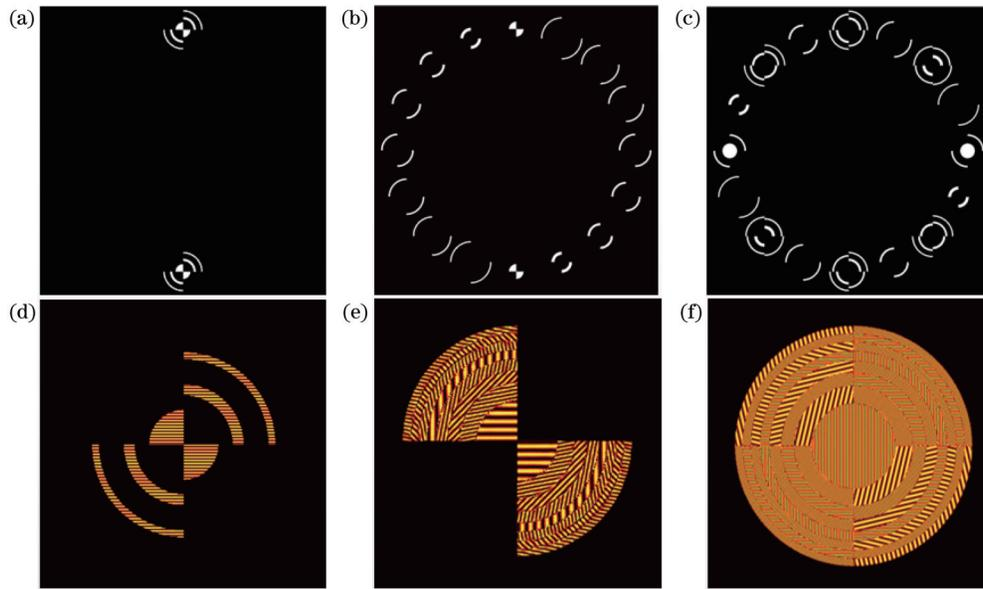


图 7 反演设计的孔径光阑及其与变取向光栅联合调制时傅里叶成像面上的光场。(a)~(c)反演设计的孔径光阑;(d)~(f)傅里叶成像面上的光场分布

Fig. 7 Inversely designed aperture diaphragms and light field distribution on Fourier imaging plane obtained by joint modulation of inversely designed aperture diaphragms and orientation-variant gratings. (a)~(c) Inversely designed aperture diaphragms; (d)~(f) light field distribution on Fourier image plane

布和多干涉光场的相干组合方式。相位元件的相对平移仅改变干涉光场的空间频率,当旋转相位元件改变透射光场取向时,需同步旋转孔径光阑。

4 实验结果与分析

与理想系统相比,实验搭建的傅里叶变换光学系统中透镜、相位元件的厚度将影响光线传播路径。在傅里叶变换光学系统中,采用的凸平面的紫外熔融石英(F_SILICA)傅里叶透镜的厚度为 5 mm,凸面曲率半径为 34.385 mm,焦距为 72.2 mm,数值孔径为

0.176。另外,所采用的熔融石英材料的相位元件的厚度为 1.5 mm。当将图 4(c)所示孔径光阑置于实际光学系统中时,系统成像面上两束相干光之间存在微小偏移,如图 8(a)所示。为消除相干光束间的偏移,利用 Zemax 优化实际光学系统中孔径光阑平面内的标准距离,优化后孔径平面的标准距离由 5.126 mm 变为 5.050 mm,此时其在系统成像面上的光场分布如图 8(b)所示。可以发现,傅里叶变换光学系统成像面上两个子光场完全重合,形成干涉光场。

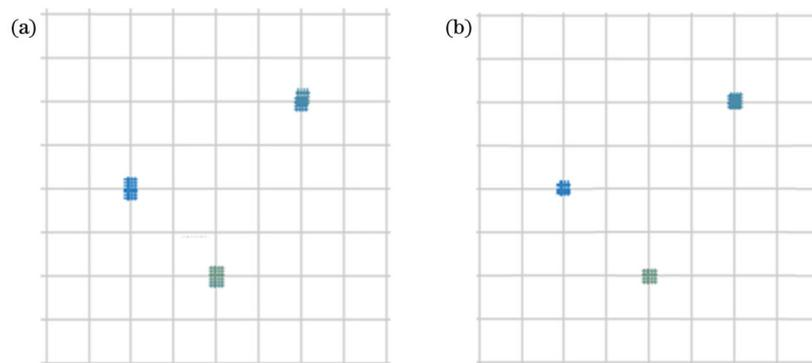


图 8 Zemax 优化前后傅里叶成像面上的光线追迹图。(a)优化前;(b)优化后

Fig. 8 Ray tracing on Fourier imaging plane before and after Zemax optimization. (a) Before optimization; (b) after optimization

实验制备了优化后的孔径光阑和相位元件,并将其置于傅里叶变换光路中,在光学系统成像面放置高分辨率光斑分析相机以检测不同调制下傅里叶成像面上的光场分布。采用图 4(b)~(d)所示的孔径光阑与空间频率为 200 lp/mm 的消 0 级光栅调制傅里叶光

学系统,当光栅相位元件分别离傅里叶频谱面 31.77、40.13、54.46 mm 时,傅里叶成像面上的光场如图 9(a)~(c)所示。每组孔径光阑均在成像面生成 3 个干涉光场,干涉光场内为栅线方向平行于水平方向的干涉条纹,三种干涉光场分布区域的边长测量值分

别为 1.712、0.902、0.330 mm。可以发现,采用反演设计制备的多像素孔径光阑与光栅相位元件调制傅里叶光学系统,其在傅里叶成像面生成的多干涉光场符合理论设计需求。当采用图 7(a)~(c)所示的孔径光阑与变参量光栅相位元件调制傅里叶光学系统时,其在傅里叶成像面上的光场分布如图 9(d)~(f)所示,多个干涉光场按照指定区域间隔或交叉分布,并可自由组

合,形成二分之一子幅面和两个子幅面拼接成的圆形光场区,其中:图 9(d)所示的各干涉光场内的干涉条纹取向相同;图 9(e)~(f)所示的各干涉光场内的干涉条纹取向不同,且图 9(e)和图 9(f)中干涉条纹的组合形式不同。可以发现,采用反演设计制备的多像素孔径光阑和变参量光栅相位元件调制傅里叶光学系统,可在傅里叶成像面上生成所需的变参量多干涉光场。

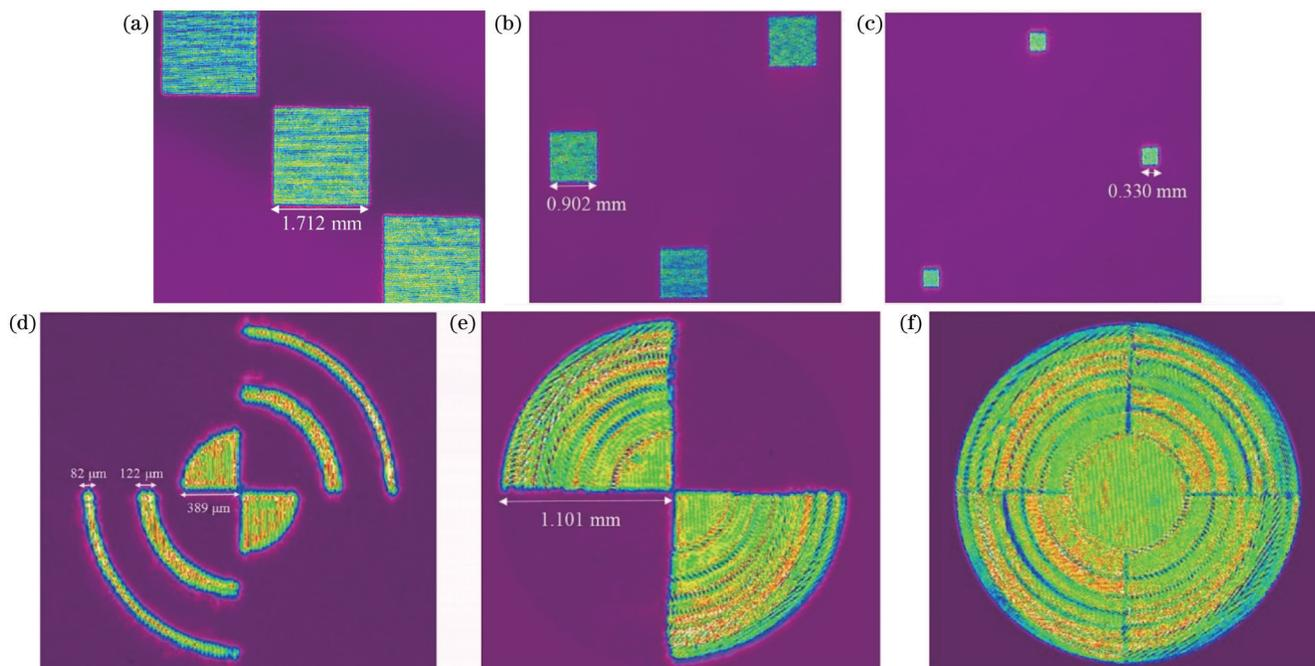


图 9 傅里叶成像面检测光场。(a)~(c)块状分布孔径光阑与光栅联合调制时的成像面光场;(d)~(f)交叉分布孔径光阑与变取向光栅联合调制时的成像面光场

Fig. 9 Detected light field on Fourier imaging plane. (a)~(c) Light field on imaging plane modulated by segmented aperture diaphragms and gratings; (d)~(f) light field on imaging plane modulated by interleaved aperture diaphragms and orientation-variant gratings

将所设计的傅里叶变换光路与双远心透镜、微缩成像物镜组成的微缩投影光路结合,在微缩成像物镜的后焦面上放置光刻胶干板,将傅里叶成像面上的光场微缩至原来的 1/12 投影至光刻胶干板上,并曝光显影记录,得到的结构如图 10(a)~(c)所示。通过对应干涉光场制备获得了分段排布的像素化纳米结构:当相位光栅离傅里叶频谱面 31.77 mm 时,其理论像素大小为 $142.0 \mu\text{m} \times 142.0 \mu\text{m}$,像素内纳米光栅周期为 473 nm;改变孔径光阑分布,平移相位元件至离傅里叶频谱面 40.13 mm 处,对应多干涉光场制备的分段排布的像素化纳米光栅像素大小为 $75.0 \mu\text{m} \times 75.0 \mu\text{m}$,像素内纳米光栅周期为 375 nm;改变孔径光阑分布,平移相位元件至离傅里叶频谱面 54.66 mm 处,对应多干涉光场制备的分段排布的像素化纳米光栅的像素大小为 $27.5 \mu\text{m} \times 27.5 \mu\text{m}$,像素内纳米光栅周期为 275 nm。因此,利用多干涉光场单次曝光可实现纳米光栅的多像素同时制备,而改变孔径光阑和平移相位元件可实现纳米光栅像素排布和光栅周期的同时调控。将上述 3 个干涉光场分时复用,在光刻胶干板

表面依次曝光,可得到不同周期的纳米结构,其对应像素以块状组合交叉分布,如图 10(d)所示,采用 3D 激光共焦显微镜测量其像素大小,对应像素测量值分别为 $142.705 \mu\text{m} \times 142.689 \mu\text{m}$ 、 $75.102 \mu\text{m} \times 75.264 \mu\text{m}$ 、 $27.576 \mu\text{m} \times 27.505 \mu\text{m}$ 。图 10(a)中像素区域内 10 个周期光栅的测量长度距离为 $4.725 \mu\text{m}$,其对应的纳米光栅周期为 472 nm,如图 10(e)所示,即实验测量值与理论值相符。

利用反演设计的多像素孔径光阑与光栅相位元件调制傅里叶变换光学系统可实现所需分段分布多干涉光场的生成与调控,并可在光敏材料表面一次干涉光刻获得多个微纳结构,为变参量微纳结构的多像素制备提供了新方法。

5 结 论

为了实现二维平面内分段、交叉分布空间变参量微纳结构的在线制备,提出了孔径光阑与相位元件联合调制的傅里叶变换光学系统,分别分析了多像素孔径光阑与相位元件、多像素孔径光阑与变参量相位元

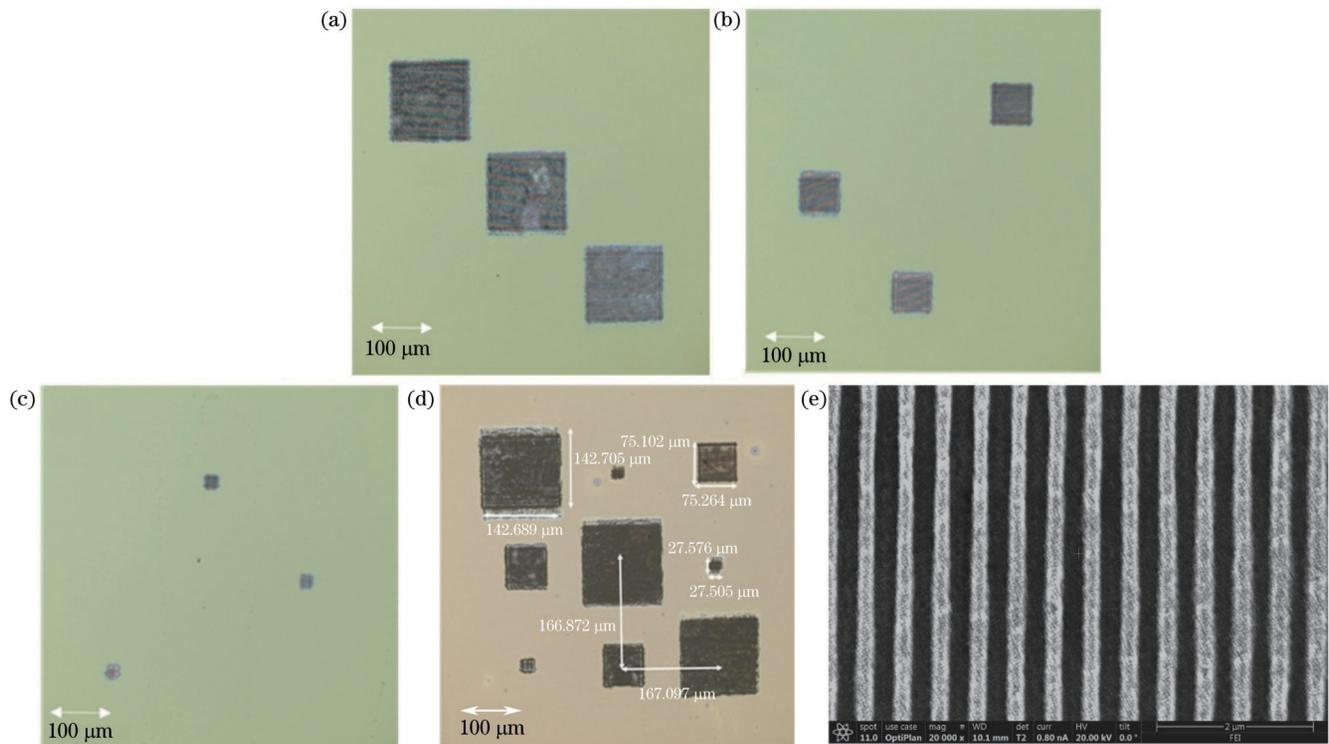


图 10 3D 激光共焦显微镜和扫描电镜测量得到的样品照片。(a)~(c) 样品照片(放大倍率为 20);(d) 空间变参量纳米结构像素测量结果;(e) 纳米光栅的扫描电镜图

Fig. 10 Sample pictures measured by 3D laser confocal microscopy and scanning electron microscopy. (a)–(c) Sample pictures (magnification of 20); (d) pixel measurement results of space-variant nanostructures; (e) scanning electron microscope image of nano-grating

件联合调制时的多干涉光场生成方法, 阐明了孔径光阑变化和相位元件相对运动对多干涉光场的调控规律。利用多像素孔径光阑与光栅联合调控, 获得了分段分布的多干涉光场。利用多像素孔径光阑与变取向光栅联合调控, 获得了交叉分布的变取向多干涉光场。利用相位元件的平移, 分时复用分段分布的多干涉光场, 在光刻胶表面上制备了像素交叉分布的变参量纳米光栅。理论与实验研究表明, 该系统可提供定制化分段、交叉分布的多干涉光场, 并可在光敏材料表面上实现变参量微纳结构的多像素制备。因此, 该系统可为多路复用或多功能超表面器件的制备提供工艺基础。

参 考 文 献

- [1] Wang S M, Wu P C, Su V C, et al. A broadband achromatic metalens in the visible[J]. *Nature Nanotechnology*, 2018, 13(3): 227-232.
- [2] Fan Z B, Qiu H Y, Zhang H L, et al. A broadband achromatic metalens array for integral imaging in the visible[J]. *Light: Science & Applications*, 2019, 8: 67.
- [3] Shalaginov M Y, An S S, Zhang Y F, et al. Reconfigurable all-dielectric metalens with diffraction-limited performance[J]. *Nature Communications*, 2021, 12: 1225.
- [4] 李勇峰, 张介秋, 屈绍波, 等. 圆极化波反射聚焦超表面[J]. *物理学报*, 2015, 64(12): 124102.
Li Y F, Zhang J Q, Qu S B, et al. Circularly polarized wave reflection focusing metasurfaces[J]. *Acta Physica Sinica*, 2015, 64(12): 124102.
- [5] Jiang Z J, Liang Q X, Li Z H, et al. A 3D carpet cloak with non-Euclidean metasurfaces[J]. *Advanced Optical Materials*, 2020, 8(19): 2000827.
- [6] Xu H X, Hu G W, Wang Y Z, et al. Polarization-insensitive 3D conformal-skin metasurface cloak[J]. *Light: Science & Applications*, 2021, 10: 75.
- [7] 宋志, 路畅, 魏国军, 等. 反射型光变色超表面滤光结构[J]. *光学学报*, 2021, 41(20): 2023001.
Song Z, Lu C, Wei G J, et al. Reflective metasurface filter with optical variable color[J]. *Acta Optica Sinica*, 2021, 41(20): 2023001.
- [8] Wu S L, Ye Y, Duan H G, et al. Large-area, optical variable-color metasurfaces based on pixelated plasmonic nanogratings[J]. *Advanced Optical Materials*, 2019, 7(7): 1801302.
- [9] Yang J H, Babicheva V E, Yu M W, et al. Structural colors enabled by lattice resonance on silicon nitride metasurfaces[J]. *ACS Nano*, 2020, 14(5): 5678-5685.
- [10] Deng Z L, Jin M K, Ye X, et al. Full-color complex-amplitude vectorial holograms based on multi-freedom metasurfaces[J]. *Advanced Functional Materials*, 2020, 30(21): 1910610.
- [11] Luo X H, Hu Y Q, Li X, et al. Integrated metasurfaces with microprints and helicity-multiplexed holograms for real-time optical encryption[J]. *Advanced Optical Materials*, 2020, 8(8): 1902020.
- [12] Bao Y J, Yu Y, Xu H F, et al. Full-colour nanoprint-hologram synchronous metasurface with arbitrary hue-saturation-brightness control[J]. *Light: Science & Applications*, 2019, 8: 95.
- [13] Iqbal S, Rajabalipanah H, Zhang L, et al. Frequency-multiplexed pure-phase microwave meta-holograms using bi-spectral 2-bit coding metasurfaces[J]. *Nanophotonics*, 2020, 9(3): 703-714.

- [14] 杨渤, 程化, 陈树琪, 等. 基于傅里叶分析的超表面多维光场调控[J]. 光学学报, 2019, 39(1): 0126005.
Yang B, Cheng H, Chen S Q, et al. Multi-dimensional manipulation of optical field by metasurfaces based on fourier analysis[J]. Acta Optica Sinica, 2019, 39(1): 0126005.
- [15] Zhang F, Pu M B, Li X, et al. All-dielectric metasurfaces for simultaneous giant circular asymmetric transmission and wavefront shaping based on asymmetric photonic spin-orbit interactions[J]. Advanced Functional Materials, 2017, 27(47): 1704295.
- [16] Chen S Q, Liu W W, Li Z C, et al. Metasurface-empowered optical multiplexing and multifunction[J]. Advanced Materials, 2020, 32(3): 1805912.
- [17] Zheng R X, Pan R H, Geng G Z, et al. Active multiband varifocal metalenses based on orbital angular momentum division multiplexing[J]. Nature Communications, 2022, 13: 4292.
- [18] Yan J X, Wang Y T, Liu Y, et al. Single pixel imaging based on large capacity spatial multiplexing metasurface[J]. Nanophotonics, 2022, 11(13): 3071-3080.
- [19] Maguid E, Yulevich I, Veksler D, et al. Photonic spin-controlled multifunctional shared-aperture antenna array[J]. Science, 2016, 352(6290): 1202-1206.
- [20] Ma M L, Li Z, Liu W W, et al. Optical information multiplexing with nonlinear coding metasurfaces[J]. Laser & Photonics Reviews, 2019, 13(7): 1900045.
- [21] Wan W P, Yang W H, Ye S, et al. Tunable full-color vectorial meta-holography[J]. Advanced Optical Materials, 2022, 10(22): 2201478.
- [22] Sun T, Hu J P, Zhu X J, et al. Broadband single-chip full stokes polarization-spectral imaging based on all-dielectric spatial multiplexing metalens[J]. Laser & Photonics Reviews, 2022, 16(6): 2100650.
- [23] Hsu W L, Chen Y C, Yeh S P, et al. Review of metasurfaces and metadevices: advantages of different materials and fabrications[J]. Nanomaterials, 2022, 12(12): 1973.
- [24] She A L, Zhang S Y, Shian S, et al. Large area metalenses: design, characterization, and mass manufacturing[J]. Optics Express, 2018, 26(2): 1573-1585.
- [25] Colburn S, Zhan A L, Majumdar A. Varifocal zoom imaging with large area focal length adjustable metalenses[J]. Optica, 2018, 5(7): 825-831.
- [26] Xu J, Wang Z B, Zhang Z A, et al. Effective intensity distributions used for direct laser interference exposure[J]. RSC Advances, 2015, 5(68): 54947-54951.
- [27] Leibovici M C R, Gaylord T K. Photonic-crystal waveguide structure by pattern-integrated interference lithography[J]. Optics Letters, 2015, 40(12): 2806-2809.
- [28] Wang K N, Zheng J H, Lu F Y, et al. Varied-line-spacing switchable holographic grating using polymer-dispersed liquid crystal[J]. Applied Optics, 2016, 55(18): 4952-4957.
- [29] Behera S, Kumar M, Joseph J. Submicrometer photonic structure fabrication by phase spatial-light-modulator-based interference lithography[J]. Optics Letters, 2016, 41(8): 1893-1896.
- [30] Liang C W, Qu T, Cai J X, et al. Wafer-scale nanopatterning using fast-reconfigurable and actively-stabilized two-beam fiber-optic interference lithography[J]. Optics Express, 2018, 26(7): 8194-8200.
- [31] Xue G P, Lu H O, Li X H, et al. Patterning nanoscale crossed grating with high uniformity by using two-axis Lloyd's mirrors based interference lithography[J]. Optics Express, 2020, 28(2): 2179-2191.
- [32] 陈林森, 乔文, 叶燕, 等. 面向柔性光电子器件的微纳光制造关键技术与应用[J]. 光学学报, 2021, 41(8): 0823018.
Chen L S, Qiao W, Ye Y, et al. Critical technologies of micro-nano-manufacturing and its applications for flexible optoelectronic devices[J]. Acta Optica Sinica, 2021, 41(8): 0823018.
- [33] 叶燕, 陈林森, 楼益民, 等. 连续可调结构光照明的超分辨显微成像方法与系统: CN105814402A[P]. 2016-07-27.
Ye Y, Chen L S, Lou Y M, et al. Super-resolution microscopy imaging method and system for continuously adjustable structured light illumination: CN105814402A[P]. 2016-07-27.
- [34] Wu S L, Ye Y, Jiang Z Y, et al. Large-area, ultrathin metasurface exhibiting strong unpolarized ultrabroadband absorption[J]. Advanced Optical Materials, 2019, 7(24): 1901162.
- [35] Wu S L, Ye Y, Gu Y, et al. Transmitted plasmonic colors with different overlays utilizing the Fano-resonance[J]. Optics Express, 2019, 27(7): 9570-9577.
- [36] Wu S L, Ye Y, and Chen L S. A broadband omnidirectional absorber incorporating plasmonic metasurfaces. Journal of Materials Chemistry C, 2018, 6(43):11593-11597.
- [37] 叶燕, 许峰川, 魏国军, 等. 实时变参量微纳光场调制系统和干涉光刻系统: CN105511074A[P]. 2016-04-20.
Ye Y, Xu F C, Wei G J, et al. Real time variable parameter micro-nano optical field modulation system and interference lithography system: CN105511074A[P]. 2016-04-20.
- [38] Ye Y, Xu F C, Wei G J, et al. Scalable Fourier transform system for instantly structured illumination in lithography[J]. Optics Letters, 2017, 42(10): 1978-1981.
- [39] Ye Y, Xu F C, Wei G J, et al. Real-time variable parameter micro-nano optical field modulation system and interference lithography system: US20180039183[P]. 2018-02-08.
- [40] 路畅, 许峰川, 许宜申, 等. 相位调制实现变参量光栅结构的干涉光刻[J]. 光学精密工程, 2022, 30(15): 1836-1844.
Lu C, Xu F C, Xu Y S, et al. Interference lithography of space-variant grating structures by phase modulation[J]. Optics and Precision Engineering, 2022, 30(15): 1836-1844.

Dynamic Multi-Interference Lithography Incorporating Modulated Optical Fourier Transform System

Ye Yan^{1,2}, Ma Yaqi^{1,2}, Song Zhi^{1,2}, Lu Chang^{1,2}, Xu Yishen^{1,2*}, Chen Linsen^{1,2**}

¹*School of Optoelectronic Science and Engineering, Collaborative Innovation Center of Suzhou Nano Science and Technology, Soochow University, Suzhou 215006, Jiangsu, China;*

²*Key Lab of Advanced Optical Manufacturing Technologies of Jiangsu Province, Key Lab of Modern Optical Technologies of Education Ministry of China, Soochow University, Suzhou 215006, Jiangsu, China*

Abstract

Objective While space-variant micro/nano structures are segmented or interleaved in a two-dimensional plane, they demonstrate integrated performance as a multi-function or multiplexing meta-device. Among present technologies, projection lithography and interference lithography are effective for the rapid fabrication of micro/nano structures. By high-resolution masks, projection lithography produces space-variant micro/nano structures quickly. However, the area of its fabricated micro/nano structures is seriously limited by variation ranges of parameters. For interference lithography, the structural profile and period can be varied by changing intensities and interference angles of light beams, respectively. Nevertheless, their corresponding micro/nano structures change in a limited range with low resolution, in addition to their complex optical setups. Combining projection lithography with interference lithography, this paper reports an optical Fourier transform system modulated by phase element to dynamically produce micro/nano structures in a wide variation range and achieves structural period variation of less than 1 nm. It merely produces structures pixel by pixel and dimension of every pixel is constant. Then, space-variant phase element is utilized as the phase element, where multi-interference light fields are generated to fabricate different micro/nano structures in different shaped pixels. However, their structural parameters and pixels cannot be customized or changed in real time. Therefore, this paper proposes a method to parallel produce micro/nano structures with independent changed structural parameters and pixels, which can be utilized to generate flexible arranged space-variant micro/nano structures for multi-function or multiplexing meta-devices.

Methods An optical Fourier transform system jointly modulated by aperture diaphragms and a phase element is proposed. With the Fourier transform principle of lenses and the geometric propagation characteristics of diffraction beams in the phase element, the generation and manipulation of multi-interference light fields in the imaging plane are discussed. The theoretical analysis shows that multi-interference light fields are determined by the distributions of aperture diaphragms and the transmission of phase elements, where the pixelated aperture diaphragms are responsible for the distribution of light fields, and the transmission of a phase element contributes to the structural parameters of each interference light fields. Furthermore, the magnification between the imaging plane and the aperture diaphragm plane as well as the one between the image plane and the transmission plane of a phase element is different, which means that the variation in aperture diaphragms and the phase element manipulates the interference light fields independently. Then, two methods for the generation and manipulation of multi-interference light fields are discussed. When modulated by multi-pixel aperture diaphragms and a phase element, multi-interference light fields are generated to parallel produce the same structure within different pixels. Pixels and the infilled structural parameters can be dynamically changed by varying aperture diaphragms and manipulating the phase elements. When modulated by multi-pixel aperture diaphragms and a space-variant phase element, multi-interference light fields are generated to simultaneously produce different structures within different pixels. The same rules are obeyed in the manipulation of the light fields except that the change in the aperture diaphragms can vary the structural pattern inside each pixel. Therefore, incorporating the analyzed methods and rules for the generation and manipulation of the interference light fields, aperture diaphragms and the phase element can be inversely designed to produce customized light fields for flexible assembled micro/nano structures.

Results and Discussions With the inversely designed methods mentioned above, symmetrical rectangular apertures are utilized as aperture diaphragms and a grating eliminating 0th transmission is acted as the phase element (Table 1) to modulate an optical Fourier transform system. Theoretical results show that three segmented interference light fields with targeted fringe frequency are produced simultaneously, while their light field distribution and interfered fringe frequency change as expected by pre-designed variation in apertures and the position of the grating (Fig. 5). Meanwhile, multi-pixel apertures and a grating with space-variant orientations are designed to modulate the Fourier transform system, and types of demand-interleaved interference light fields are generated for the fringes with their orientations flexibly arranged (Fig. 7). Experimentally, aperture diaphragms and phase elements fabricated as designed are placed in the optical Fourier transform

system, and segmented/interleaved interference light fields, coincident with the theoretical ones, are detected in its imaging plane (Fig. 9). Combining the multi-interference light fields with the miniature projection, arrays of segmented nano-gratings are fabricated consequently. With the time division multiplexing of dynamically controlled multi-interference light fields, segmented nano-gratings of nine pixels are fabricated with measured pixel dimensions of $142.705\ \mu\text{m} \times 142.689\ \mu\text{m}$, $75.102\ \mu\text{m} \times 75.264\ \mu\text{m}$, $27.576\ \mu\text{m} \times 27.505\ \mu\text{m}$ as well as structural periods of 472 nm, 375 nm and 275 nm (Fig. 10).

Conclusions Incorporating planar segmented or interleaved space-variant micro/nano structures, meta-device demonstrates multi-function or multiplexing performance. To fabricate customized distributed and space-variant micro/nano structures with interference, this paper proposes an optical Fourier transform system, which is jointly modulated by aperture diaphragms and a phase element. With the Fourier transform principle of lenses and the geometric propagation characteristics of diffraction beams in the phase element, the methods for the generation and manipulation of flexibly distributed multi-interference light fields in the imaging plane are analyzed. Apertures and a grating, as well as apertures and a grating with space-variant parameters, are inversely designed as aperture diaphragms and a phase element respectively to obtain the required distribution of variant micro/nano structures. Theoretical and experimental results verify that with the inversely designed aperture diaphragms and the phase element modulating the optical Fourier transform system, target interference light fields for arrays of segmented or interleaved micro/nano structures can be realized. Combined with the multi-interference light fields and the miniature projection, arrays of segmented nano-gratings are fabricated in sequence. With the time division multiplexing of dynamically controlled multi-interference light fields, nano-gratings with three periods are fabricated segmentally, which shows great potential for the rapid fabrication of multi-functional meta-devices.

Key words optical design; phase modulation; $4f$ optical system; space-variant structure; interference lithography